Econ. Environ. Geol.
Vol. 31, No. 1, p. 21-29, 1998.

Crustal Structure of the Korean Peninsula from Broadband Teleseismic Records by Using Receiver Function

So Gu Kim*, Seoung Kyu Lee*, Myung soon Jun and Ik Bum Kang****

ABSTRACT : Broadband receiver functions are developed from teleseismic P waveforms recorded at Wonju (KSRS), Inchon (IRIS), and Pohang (PHN), and are analyzed to examine the crustal structure beneath the three stations. The teleseismic receiver functions are inverted in the time domain to the vertical P wave velocity structure beneath the stations. Clear P-to-S converted phases from the Moho interface are observed in teleseismic seismograms recorded at the three stations. We estimated the crustal velocity structures beneath the stations using the receiver function inversion. The general features of inversion results are as follows: (1) For Pohang station, there is a high velocity gradient at a 4~5 km deep for SE and NW back azimuth and a low velocity zone at around 10 km deep. The Moho depth is 28 km for NW direction. (2) The shallow crustal structure beneath Wonju station is somewhat complex and there is a high-velocity zone ($V_p \simeq 6.8$ km/sec) at 3 to 4 km deep. The average crustal thickness is 33 km, and a transition zone exists at a 30~33 km deep of lower crust, of which velocity is abruptly changed 6.4 to 7.9 km/sec. (3) For Inchon station, the crustal velocity gradient monotonously increases up to the Moho discontinuity and the velocity is abruptly changed from 6.2 km/sec to 7.9 km/sec at 29 km deep.

Introduction

Considerable interests in the structure of the crust and upper mantle have been generated by the recent papers of Helmberger, Wiggins (1971), Burdick, Langston (1977), Langston (1977a; 1977b; 1979), Owens *et al.* (1984; 1987), Liu, Kind (1987), Priestly *et al.* (1988), Owens (1987), Owens, Crosson (1988), Ammon *et al.* (1989, 1990), McNamara, Owens (1993), Zhu *et al.* (1995), and many others. Regnier (1988) has used deep focus (depth > 117 km) events to study a lateral variation of upper mantle structure beneath New Caledonia. The models that have been proposed by these authors show many similarities but differ subs- tantially in detail. It has been shown that the converted phases can be used not only for determining the depth of discontinuities in the earth, but also for investigating their lateral fluctuations. A specific converted phase within the body wave train is associated with a specific interface and its time delay mainly on the depth and structure of the interface underneath the receiver.

A previous study on the crustal structure in the Korean Peninsula is poor. So we will precisely examine the crustal structure of the Korean Peninsula using teleseismic P waveforms for three stations which are located at Wonju station (central eastern part), Inchon (central western part), and Pohang station (southeastern part), respectively. This study will be presented in two parts. First, a general method for equalizing the wave form data for arbitrary effective source time function will be discussed. Second, the equalized P waveform data will be interpreted by calculating theoretical ray amplitudes and synthetic seismograms computed with the method proposed by Langston (1977b). We also model receiver functions obtained from teleseismic P waveforms recorded at three sites, Wonju, Inchon, and Pohang, to determine the detailed structure of the crust and upper mantle directly beneath the recording sites. The broadband receiver function method is most sensitive to the details of vertical shear velocity distribution in the crust. In this paper we have attempted to determine the vertical P velocity distributions by using the receiver function inversion method proposed by Ammon *et al.* (1990).

* The Seismological Institute, Hanyang University, Ahnsan, Kyonggi-do 425-791, Korea
** Korean Institute of Geology, Mining and Materials, Daejon 305-350, Korea

Fundamental methods of receiver functions

The method is based on the identification of converted or multiply reflected phases within the first 10 seconds of the P-wave arrivals. These phases are used to determine the interface depth and velocity distribution within the lithosphere beneath a station. Lateral inhomogeneities of the lithosphere may be

derived by observational and theoretical studies. There are several Ps converted phases within the first 10 seconds of the direct teleseismic P wave train which can be identified on the rotated SV component. The common features of the Ps converted phases are described as follows:

1) The time delays of phases converted at shallow structures depend mainly on the receiver structure, on the other hand the effects of epicentral distances are small.

2) The energy of Ps conversions is closely associated with an interface structure where the incoming wave is converted.

3) Ps conversions are identified where acoustic impe- dances are quite different. The Ps waveforms are generally quite similar to those ones of the original P-wave. They are used to calculate the depth of sedimentary layer and Moho discontinuity.

A data processing procedure is performed to improve the identification of the Ps conversion. The first step is to rotate horizontal components to the theoretical radial and tangential components. Because the angles of incidence for teleseismic P waves are nearly vertical, we can observe the pulse-like or impulsive P wave forms from the teleseismic or deep focus earthquakes. Likewise, P to SV converted phases at boundaries within the structure will be polarized nearly horizontally and, thus, be predominant on radial component. Using this phenomenon, we can calculate the response of the crust and upper mantle velocity structure, termed the receiver functions. In order to obtain receiver function, we must remove the source, path, and instrument effects which also influence the recorded seismograms. Therefore we first select earthquakes which have the same source and station for the sake of equalization. We are primarily interested in direct P-to-S converted wave and the first P crustal reverberation phases (PpPms, PpSms). The horizontal components of the receiver functions are isolated using a deconvolution procedure (Langston, 1979). In this process, we use the vertical component ($D_V(t)$) and the rotated $D_R(t)$ and $D_T(t)$ components to calculate receiver functions. This approach assumes that the vertical component contains primarily the unwanted source and path effects. The source equalization method of Langston (1979) can be theoretically represented by

$$\begin{aligned} D_{V(t)} &= I(t) * S(t) * E_V(t) \\ D_R(t) &= I(t) * S(t) * E_R(t) \\ D_T(t) &= I(t) * S(t) * E_T(t) \end{aligned} \quad (1)$$

where subscripts *V, R,* and *T* represent vertical, radial, and tangential components, respectively. *I(t), S(t),* and *E(t)* are the impulse response of the recording instrument, the seismic source function, and the impulse response of the earth structure, respectively. Asterisks represent the convolution operator. Generally, the horizontal components are quite different from the vertical component because the earth structure beneath a station will generate phase conversions of the P-to-S type. The source equa- lization scheme assumes that

$$E_V(t) \approx \delta(t)$$

where $\delta(t)$ is the *Dirac delta* function.

$$D_V(t) \approx I(t) * S(t) \quad (2)$$

We can remove the impulse response of the recording instrument and the source and path effect from our observed seismograms through the source and path equalization procedure, so that isolating $E_R(t)$ and $E_T(t)$ can be accomplished by deconvolving, respectively.

The procedure for performing this deconvolution in frequency domain is to divide the the horizontal component by the vertical component after introducing a minimum allowable amplitude level for the amplitude spectrum of the vertical component. The deconvolved seismograms are convolved with a Gaussian time function to produce a smoothing and wave-shaping of horizontal receiver functions as follows:

$$\begin{aligned} E_R(\omega) &= \frac{\overline{D}_V(\omega) D_R(\omega)}{\Phi(\omega)} G(\omega) \\ E_T(\omega) &= \frac{\overline{D}_V(\omega) D_T(\omega)}{\Phi(\omega)} G(\omega) \end{aligned} \quad (3)$$

where, $\Phi(\omega) = Max\ \{ [D_V(\omega)\ \overline{D}_V(\omega),\ c\ Max\ [D_V(\omega)\ \overline{D}_V(\omega)]\}$ means autocorrelation of $D_V(\omega)$, and c is a value of water level and chosen for the value which produced the highest-quality. In most cases we found c=0.001 for INCN and KSRS data and c=0.01 for PHN data. $G(\omega) = \exp^{-\omega^2/4\alpha^2}$, α controls the width of the Gaussian pulse, and the bar over $D_V(\omega)$ indicates its complex conjugate. α (2.5 for PHN, 4.0 for INCN, KSRS) used in this paper means passband filter. The α and c values are important factors to construct receiver functions. The source equalization technique produces horizontal receiver functions which are similar even for events with quite different source functions.

The second step is to derive a vertical velocity structure model using the stacked receiver functions. At first, we should choose a *priori* model for each stations using a forward modeling technique pro-

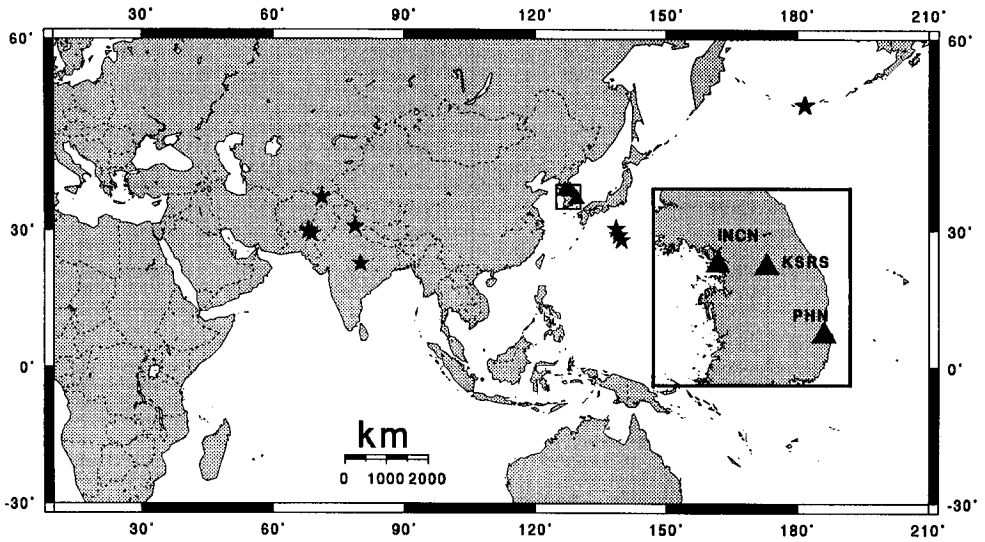

Fig. 1. Map showing three stations (closed triangles) and teleseismic and deep focus events (closed asterisks). INCN (IRIS station at Inchon), KSRS (at Wonju), and PHN (POSEIDON station at Pohang).

posed by Langston (1977b). The receiver functions obtained from broadband data are usually much too detailed to be effectively analyzed using forward model technique (Owens, 1987). Therefore, we used the linearized time domain waveform inversion method proposed by Ammon *et al.* (1990) of which algorithms are improved with the modified fast partial derivatives of Randall (1989) and included a smoothness constraint on all the resulting velocity models utilizing the "Jumping" inversion technique of Shaw, Orcutt (1985). The receiver function inversion scheme of Ammon *et al.* (1990) consists of a linearized-iterative, least-squares waveform fitting. The algorithm has a merit of which computational efficiency coupled with a implementation of smoothness constraint allows for more flexible models and the methods are applied to minimize the energy in the second difference of the model parameters. To compute modeled receiver functions for a given velocity structure, a technique based on propagator matrix method is used (Kennett, 1983). In this study, we assumed $V_P=\sqrt{3}V_S$ and density $\rho=0.32V_P+0.77$ (Berteussen, 1977), where ρ (g/cm^3) represents density, V_P and V_s (km/sec) represent the P and S velocity assuming a Poisson's ratio of 0.25.

Data Analysis

In this study, the broadband 3-component data recorded at Pohang, Inchon, and Wonju stations are used. Fig. 1 shows the seismic stations and teleseismic event locations used in this study. The KSRS and IRIS data are recorded with a sampling rate of 20 sps (samples per second), the PHN data is recorded with a sampling rate of 10 sps. All of them are broadband velocity seismograms. For Pohang station, we tried to find deep focus ($\triangle \leq 10°$, depth $\simeq$ 440 km) and teleseismic events to avoid multiple

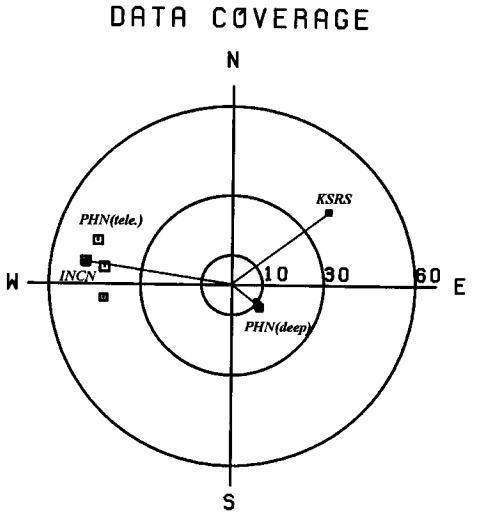

Fig. 2. Teleseismic data coverage at Inchon, Wonju, and Pohang stations. The size of symbol indicates a difference of event magnitudes. Events used in stacked receiver functions are listed in Table 1. The numbers are epicentral distances in degree.

Table 1. Seismic parameters for teleseismic and deep focus events for receiver function analysis.

Stations	DATE m/d/yr	O.T.(UT) h:m:s	Distance (deg)	BAZ (deg)	Epicenter Lat.	Epicenter Lon.	Depth (km)	Mag. (mb)
INCN	2/27/97	21:8:2.40	48.60	279.20	29.90	68.10	6.0	6.5
	2/27/97	21:30:36.60	48.70	279.40	30.01	67.98	33.0	6.1
	3/4/97	13:3:47.00	48.30	278.20	29.36	68.82	33.0	5.9
	5/21/97	22:51:28.90	42.30	263.90	23.18	80.02	32.0	6.1
KSRS	8/19/96	4:19:15.60	39.90	51.90	51.43	-178.45	33.0	5.7
	8/31/96	20:47:23.00	40.00	51.90	51.41	-178.23	33.0	5.8
PHN	5/3/91	2:14:14.40	11.70	129.60	28.08	139.58	433.0	6.0
	7/29/95	16:18:44.80	9.40	124.30	30.35	138.38	436.0	5.6
	3/16/96	22:4:6.20	10.70	128.30	28.98	138.94	477.0	5.9
	7/14/91	9:9:11.90	46.40	288.50	36.33	71.11	212.0	6.4
	10/19/91	21:23:14.30	42.20	277.90	30.78	78.77	10.0	6.5

phases in the source time function (Regnier, 1988). Fig. 2 shows the clusters of the teleseismic data for Inchon, Wonju, and Pohang stations. The detailed parameters of the earthquakes are listed in Table 1. We calculated theoretical back azimuth and incidence angle of receiver area by using EDABAC (II) software (Herrmann, 1994).

We used the deconvolution procedure proposed by Langston (1979) to isolate the response of the structure beneath the stations from the source and path effects. For teleseismic recorded at 30° to 90° and a deep focus events, the initial energy arriving from the source region consists of plane P-wave arrivals. In general, all of the teleseismic waves will produce P to S conversion and direct P reverberations beneath the stations, and horizontal components of ground motions are quite different from the vertical component (Owens, 1987; Priestley *et al.*, 1988). We can obtain the radial receiver function by deconvolving the vertical from the radial seismogram. The receiver functions from the events clustered both in distance and in back azimuth are then stacked in the time domain to obtain a single estimate of the horizontal receiver function. The stack result from the individual receiver functions shows a little difference and is much improved with the high signal-to-noise ratios. In Fig. 3a and 3b, individual and stack radial receiver functions are shown for INCN, KSRS stations, and Fig. 3c and 3d show radial receiver functions of deep focus and teleseismic events for PHN station. The consistency of the Moho Ps phase can be seen at 3.8~4.0 seconds after the direct P arrival from receiver functions. Seismograms are labeled with event station, date, and back azimuth. The stack receiver functions were inverted using a linearized inversion procedure (Owens *et al.*, 1984) with the modified fast partial derivatives method of Ammon *et al.* (1990).

The earth structure is parameterized by a series of plane horizontal layers, and iterative procedure is used to minimize the residuals between the observed radial receiver function and the synthetic predicted by a modelled structure. Our initial simple models are determined by a receiver function forward model. To determine the simple initial model, we tested arrival times of each phase (Moho Ps and direct conversion Ps phases) using previous velocity models (Kim, Kim, 1983; Kim, Lee, 1994). Three initial models consist of a 4 or 5 layered structure. For Inchon station, the initial model is modified from Kim, Kim (1983). For Wonju station, the initial model is modified from Kim, Lee (1994). For Pohang station, the initial model is made with low velocity layer (8 km thickness) at 38 km deep which is largely modified from Kim, Kim (1983). For the inversion model tests, we parameterized thin layer (0.5 km or 1.0 km thick) for shallow structure (0~15 km deep) and parameterized thick layer (2.0 or 3.0 km thick) below 15 km depth and increased velocity with depth for three stations. Fig. 4 shows the inversion results for 280° back azimuth at Inchon station. Final (thick solid) and initial (thick dotted) velocity models, and iterative velocity models (thin solid) are well converged to final model (upper part). The synthetic radial receiver function (thin dotted) compared to the stack one (thick solid) is well fitted (lower part).

Fig. 5 shows the inversion results for 52° back azimuth at Wonju station in the same manner Fig. 4. Fig. 6 shows the inversion results using deep focus events for 140° back azimuth at Pohang station as Fig. 4. Fig. 7 shows the inversion results using teleseismic events for 290° back azimuth at Pohang station as Fig. 4. The LVZ (lower velocity

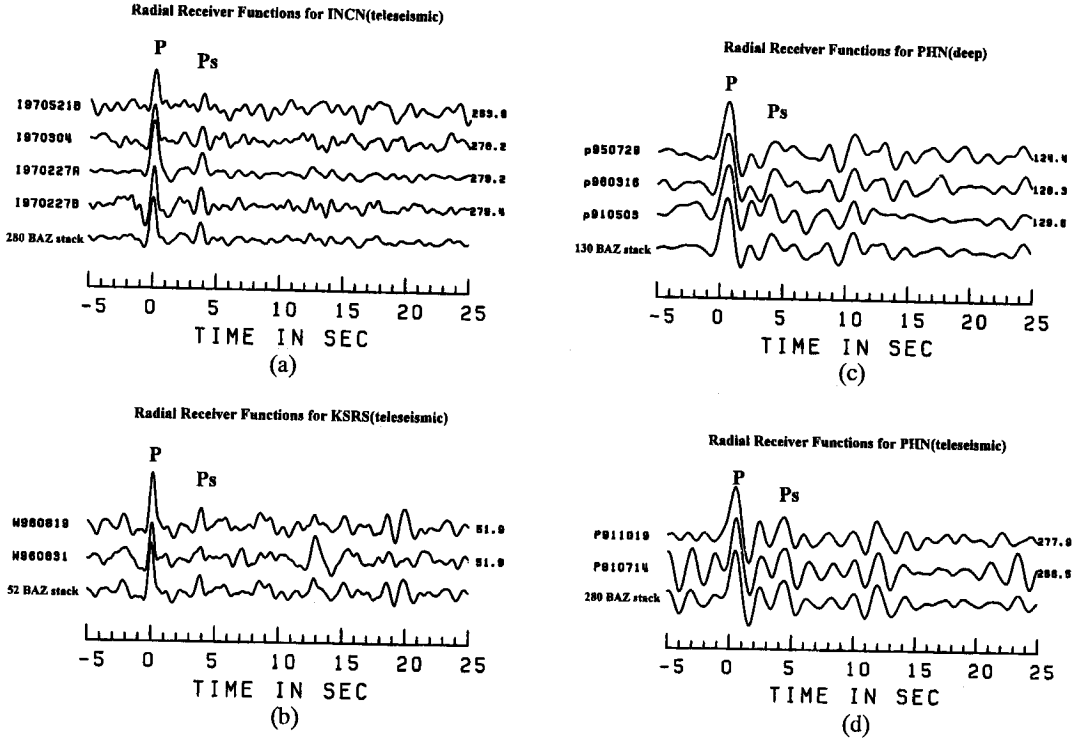

Fig. 3. (a) The individuals and stack radial receiver functions at INCN stations for 280° back azimuth. The consistency of the Moho Ps phase approximately 3.8~3.9 seconds after the direct P arrival and also see the direct P wave multiples at 10~20 sec. Left numbers indicate that the first letter means station and the other numbers are events date, right number indicates back azimuth, (b) The individuals and stack radial receiver functions at KSRS stations for 52° back azimuth. The consistency of the Moho Ps phase approximately 3.8~3.9 seconds after the direct P arrival and also see the direct P wave multiples between 12 sec and 20 sec. The number means as Fig. 3a, (c) The individuals and stack radial receiver functions at PHN stations for 130° back azimuth are deep focus events. The consistency of the Moho Ps phase approximately 4.3 seconds after the direct P arrival (0.5 sec) and also see the direct P wave multiples at 8 sec and 14 sec. The number means as Fig. 3a, (d) The individuals and stack radial receiver functions at PHN stations for 280° back azimuth are teleseismic events. The consistency of the Moho Ps phase approximately 4.4 seconds after the direct P arrival (0.4 sec) and also see the direct P wave multiples at 10~15 sec. The number means as Fig. 3a.

zone) at 10 km deep can be seen for 280° back azimuth. Fig. 8 shows the final velocity models of three stations which are derived from the inversion results.

To investigate the depth-velocity trade-off, we analyzed the sensitivity of a layer over a half-space model to variations in velocity of the layer, while keeping the amplitudes of the receiver function arrivals constant. The theoretical receiver function corresponding to a layer over a half space may be expressed as follows (Ammon *et al.*, 1990):

$$R_{(t)} = \sum_{i=0}^{n} a_i s\,(t - \tau_i) \qquad (4)$$

where $\boldsymbol{R(t)}$ represents the receiver function, a_i represents the amplitude and τ_i represents arrival time of ith arrival relative to the direct P wave. $s(t)$ represents the source time function of a Gaussian pulse which is $s(t)=\exp(-gt^2)$ with Gaussian width factor g (selectable values). The amplitudes a_i depend on the shear velocity, Poisson's ratio, and density of both the layer and half-space. The travel times τ_i depend only on the shear velocity, Poisson's ratio, and layer thickness h.

The estimate of the receiver function is described by

$$R^{est}(t) = \sum_{i=0}^{n} a_i s\,(t - \hat{\tau}_i) \qquad (5)$$

where $\hat{\tau}_i$ represents the estimated travel time of the ith ray. We measure the error in waveform fit by

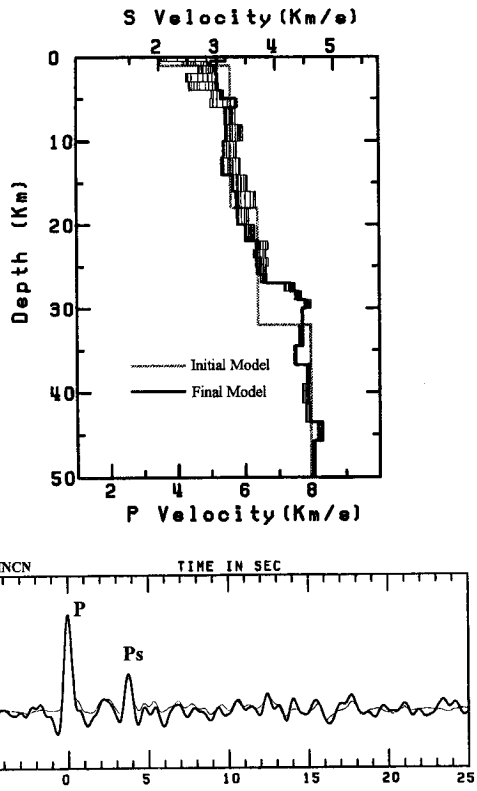

Fig. 4. Inversion results for 280° back azimuth at INCN station. (upper) Final (thick solid) and initial (thick checked) velocity models, and iterative velocity models (thin solid) are well converged to final velocity model. (lower) Synthetic radial receiver function (thin dotted) compared to observed stack (thick solid) radial receiver functions is well fitted.

summing the squares of residual vector $r(t)$:

$$r(t) = \sum_{i=0}^{n} \{R^{obs}(t_i) - R^{est}(t_i)\} \quad (6)$$

where $R^{obs}(t)$ represent the reference waveform which is a mean stacked receiver function.

By examining the inversion results from the thin-layer to identify the depths of the significant seismic impedance contrasts (velocity, density), the final depth-velocity models of three stations were determined. The waveform fit residuals of all the models are estimated to be less than 4%, indicating that the models are reasonable.

Results and Discussion

The waveform fit residuals using the Eq. (6) are less than 4% for each station. The Wonju and

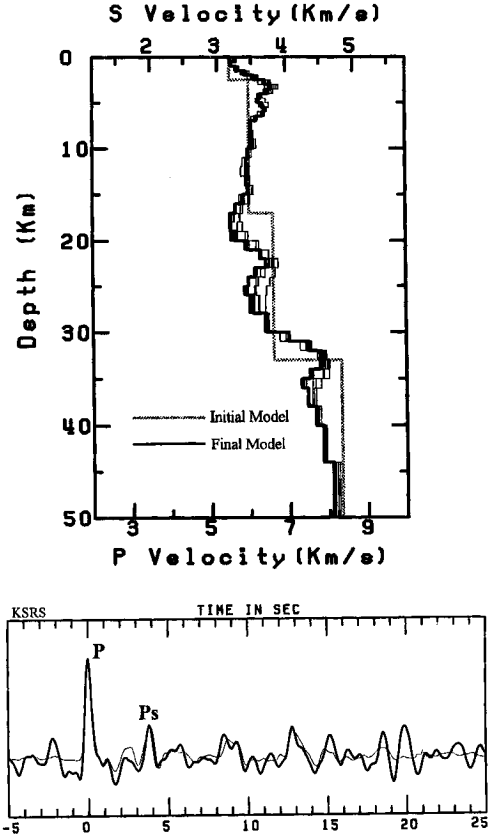

Fig. 5. Inversion results for 52° back azimuth at KSRS station. Same display scheme as Fig. 4.

Inchon stations are located in the central parts of the Korean Peninsula, and The Pohang station is located at the southeastern part of the Korean peninsula. The geological structure of the Pohang station is different from the other stations. The seismotectonics of Pohang area are the Cenozoic depression and graben (Kim, Gao, 1995) which include the Kyongsang Sedimentary Basin. On the other hand, the seismotectonics of Inchon and Wonju station consist of Kyonggi sedimentary layer of the platforms with strike N50°E (Lee, Kim, 1990). The P velocity beneath the Inchon station is linearly increased from the surface up to 27 km deep, and the P-wave velocity is rapidly increased from 6.2 km/sec to 7.9 km/sec at 29 km in depth. From this inversion result, the Moho discontinuity may exist at a 29 km deep. For Wonju station, the P velocity of shallow crustal structure is rapidly increased from 5.6 km/sec at surface to 6.5 km/sec at 4 km deep, the low velocity layer may exist from 18 km to 22 km deep. From 30 km to 32 km deep, the P velocity is rapidly increased 6.2 km/sec to 7.9 km/sec. The Moho

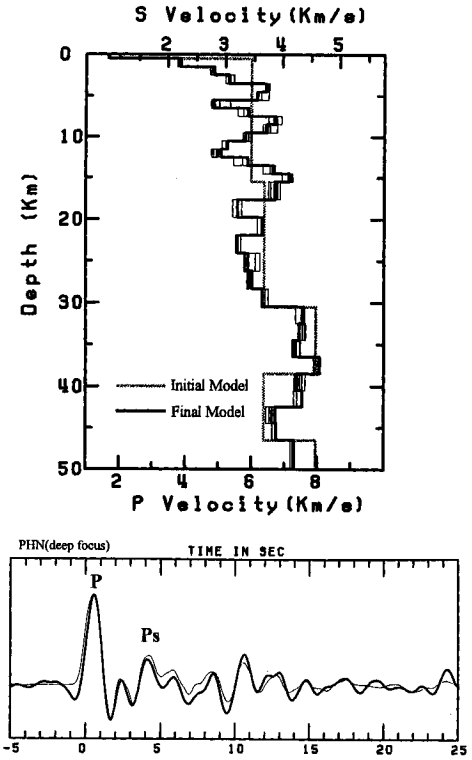

Fig. 6. Inversion results using deep focus events for 130° back azimuth at PHN station. Same display scheme as Fig. 4.

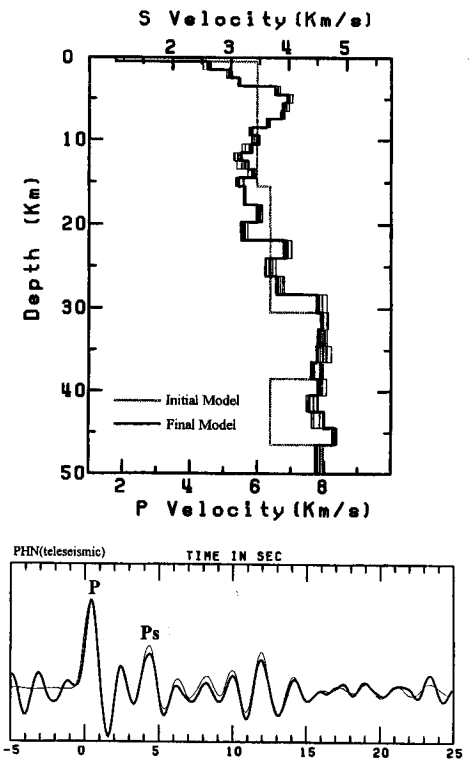

Fig. 7. Inversion results using teleseismic events for 280° back azimuth at PHN station. Same display scheme as Fig. 4.

discontinuity is estimated as about 33 km deep. For Pohang station, two velocity models are determined. The one is of the deep focus events for 130° back azimuth and the other is of the teleseismic events for 280° back azimuth. For deep focus events, the P velocities increase from 1.8 km/sec at surface to 5.4 km/sec at 4 km deep. This layer consists of a high velocity rock of basin. It is hard to explain the tendency of the velocity variations by only using this result. For the inversion result from the teleseismic events for 280° back azimuth, the shallow velocity structure (< 4 km) is the same as the results using deep focus events.

The depth of the Moho discontinuity is about 29 km at Inchon station for 280° back azimuth, and about 33 km at Wonju for 52° back azimuth, respectively. For Pohang station, the velocity models are somewhat complex from 5 km to 28 km deep in which velocity is changed from 4.8 to 7.2 km/sec, the depth of the velocity discontinuity (7.4 km/sec) for deep focus (130° back azimuth) is about 30 km. On the other hand, for the teleseismic events the depth of the Moho discontinuity (V_p=7.9 km/sec) is about 28 km in the

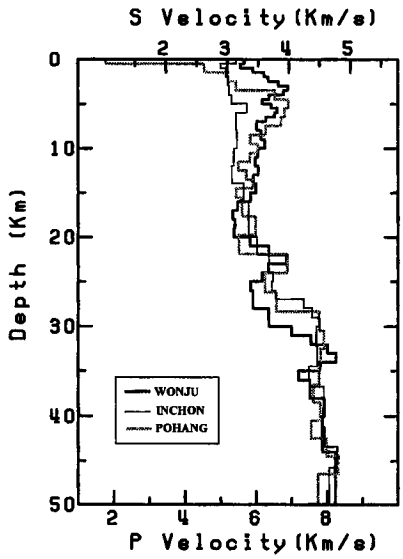

Fig. 8. Comparisons of the velocity models among the Inchon (NW direction), Wonju (NE direction), and Pohang (NW direction) stations which are results from the receiver function inversions.

direction of 280°.

Conclusions

The depth of the Moho discontinuity beneath the Pohang, Wonju, and Inchon stations are estimated to be 28 km for NW (280° back azimuth) direction, 33 km for NE (52° back azimuth) direction, and 29 Km for NW (280° back azimuth) direction, respectively.

1) The general features of inversion results for the Pohang station indicate that the high velocity gradient at 4 km deep appears for SE and NW directions. The crustal structure of SE direction is somewhat complex. On the other hand, for NW direction, the Moho discontinuity is assumed at 28 km deep and a crustal low-velocity zone (LVZ) exists at near 10 km deep.

2) P-wave velocity of the shallow crust (5.8 to 6.8 km/sec) of Wonju station is rapidly increased and the most prominent structure is a high-velocity zone (P velocity=6.8 km/sec) at 3 to 4 km of a shallow structure. The transition zone exists at a 30-33 km deep of lower crust of which velocity is abruptly increased 6.4 to 7.9 km/sec.

3) For Inchon station, the crustal velocity gradient monotonously increases up to the Moho discontinuity and the velocity is abruptly changed from 6.2 km/sec to 7.9 km/sec at 29 km deep.

The above velocity models and synthetic test results indicate that a receiver function inversion images velocity discontinuities and a depth-velocity ratio (similar to deep seismic refraction studies), not absolute velocity structure (Ammon *et al.*, 1990).

Acknowledgements

This study was supported by the Korean Ministry of Education (BSRI-96-5420) and the Korea Research Foundation (96). The research was also partly financed by the Korea Institute of Geology, Mining and Materials (KIGAM) and the Korea Atomic Energy Research Institute (KAERI).

References

Ammon, C.J., Zucca, J., and Kasameyer, P. (1989) An S-to-P converted phase recorded near Long Valley/Moho Craters Region, California. J. Geophys. Res., v. 94 (B12), p. 17721-17727.

Ammon, C.J., Randall, G., and Zandt, G. (1990) On the nonuniqueness of receiver function inversions. J. Geophys. Res., v. 95 (B10), p. 15303-15318.

Berteussen, K.A. (1977) Moho depth determinations based on spectral ratio analysis of NORSAR long-period P waves. Phys. Earth Planet. Inter., v. 31, p. 313-326.

Burdick, L.J. and Langston, C.A. (1977) Modeling crustal structure through the use of converted phases in teleseismic body-wave forms. Bull. Seism. Soc. Am., v. 67, p. 677-691.

Haskell, N. A. (1962) Crustal reflection plane P and SV waves. J. Geophys. Res., v.67, p.4751-4767.

Helmberger, D. and Wiggins, R.A. (1971) Upper mantle structure of midwestern United States. J. Geophys. Res., v. 76 (14), p. 3229-3245.

Herrmann, R.B. (1994) Computer Programs in Seismology. Saint Louis University.

Kim, S.J. and Kim, S.G. (1983) A study on the crustal structure of south Korea by using seismic waves. J. Korean Inst. Mining Geol., v. 16, p. 51-61 (in Korean).

Kim, S.G. and Lee, S.K. (1994) Crustal modelling for the southern parts of the Korean Peninsula using observational data and ray method. Kor. Inst. Min. and Energ. Res., v. 31, p. 549-558 (in Korean).

Kim, S.G. and Gao, F. (1995) Korean Earthquake Catalogue. The Seismological Institute of Hanyang University.

Kennett, B.L.N. (1983) Seismic Wave Propagation in Stratified Media. Cambridge University Press, New York, p. 342.

Langston, C.A. (1977a) Corvallis, Oregon, crustal and upper mantle receiver structure from teleseismic P and S waves. Bull. Seism. Soc. Am., v. 67, p. 713-724.

Langston, C.A. (1977b) The effect of planar dipping structure on source and receiver responses for constant ray parameter. Bull. Seism. Soc. Am., v. 67, p. 1029-1050.

Langston, C.A. (1979) Structure under Mount Rainier, Washington, inferred from teleseismic body waves. J. Geophys. Res., v. 84(B9), p. 4749-4762.

Lee, D.Y. and Kim, J.Y. (1990) Quaternary Geology of the Pohang-Youngil Area. KIER-Research Report (KR-90-1A-2).

Liu, Q. and Kind, R. (1986) Lateral variations of the structure of the crustal-mantle boundary from conversions of teleseismic P waves. J. Geophysics, v. 60, p. 149-156.

McNamara, D.E. and Owens, T.J. (1993) Azimuthal shear wave velocity anisotropy in the basin and range province using moho Ps converted phases. J. Geophys. Res., v. 98(B7), p. 12003-12017.

Owens, T.J., Zandt, G. and Taylor, S.R. (1984) Seismic evidence for an ancient rift beneath the Cumberland Plateau, Tennessee: A detailed analysis of broadband teleseismic P waveforms. J. Geophys. Res., v. 89(B9), p. 7783-7795.

Owens, T.J., Taylor, S.R. and Zandt, G. (1987) Crustal structure at regional seismic test network stations determined from inversion of broadband teleseismic P waveforms. Bull. Seism. Soc. Am., v. 77, p. 631-662.

Owens, T.J. (1987) Crustal structure of the Adirondacks determined from broadband teleseismic waveform modeling. J. Geophys. Res., v. 92 (B7), p. 6391-6401.

Owens, T.J. and Crosson, R.S. (1988) Shallow structure effects on broadband teleseismic P waveforms. Bull. Seism. Soc. Am., v. 78, p. 96-108.

Priestly, K.F., Zandt, G. and Randall, G.E. (1988) Crustal structure in Eastern Kazakh, U.S.S.R. from teleseismic receiver functions. Geophys. Res. Lett., v. 15, p. 613-616.

Regnier, M. (1988) Lateral Variation of Upper Mantle structure

beneath New Caledonia determined from P-wave receiver function: evidence for a fossil subduction zone. Geophysical Journal Int., v. 95, p. 561-577.

Shaw, P.R., and Orcutt, J.A. (1985) Waveform inversion of seismic refraction data and applications to young Pacific crust. Geophys. J.R. Astron. Soc., v. 82, p. 375-414

Zhu, L., Owens, T.J. ,and Randall, G.E. (1995) Lateral variation in crustal structure of the northern Tibetan Plateau inferred from teleseismic receiver functions. Bull. Seism. Soc. Am., v. 85, p. 1531-1540.

Manuscript received 15 October 1997

광대역 원격지진의 수신함수를 이용한 한반도 지각구조

김소구 · 이승규 · 전명순 · 강익범

요 약 : 원주 (KSRS), 인천 (IRIS), 그리고 포항 (PHN)에서 관측한 원격 지진 P파로부터 광대역 수신 함수 (Receiver Function)를 이용하여 관측소 하부의 지각 속도 모델을 찾았다. 3개의 관측소에서 기록된 수신 함수 파형으로부터 모호 불연속면에서 전환된 Ps파형을 명확하게 관측할 수 있었다. 각 관측소에서 관측된 수신 함수들은 신호 대 잡음 비 (S/N ratio)를 향상시키기 위해 후방위각과 진앙 거리가 거의 같은 수신 함수들끼리 스태킹 (Staking)하였다. 이와 같이 스태킹한 수신함수를 수신함수 역산법 (Receiver Function Inversion Method)을 이용하여 다음과 같은 결과를 얻었다: (1) 포항 관측소에는 후방위각 남동 (SE)과 북서 (NW)방향의 수신 함수 역산 결과 표층으로부터 4~5 km에서 고속도층이 존재하며 10 km깊이부터 저속도층 (LVZ)이 존재하고 있다. 그리고 북서 (NW)방향의 원격 수신 함수 역산 결과 약 28 km 깊이에 모호 불연속면이 존재하는 것을 찾았다. (2) 원주 관측소에서는 북동 (NE)방향의 원격 수신 함수 역산 결과 천부 지각 속도 구조 양상이 다소 복잡하고 3~4 km깊이에 고속도대 (high-velocity zone, $V_p \simeq 6.8$ km/sec)가 존재하는 것으로 나타났다. 이 지역의 평균 지각 두께는 33 km이며, 30~33 km깊이에서 속도가 6.4 km/sec 에서 7.9 km/sec로 급격히 변하는 지각-맨틀 경계가 존재하는 것을 알 수 있다. 따라서 Moho 불연속면의 깊이는 33 km로 추정된다. (3) 북서 (NW)방향의 수신함수 분석결과 인천 관측소 하부의 지각 속도 모델의 특징으로는 P파의 속도는 표층부터 선형적으로 증가되고 또한 26~29 km 깊이에 P파 속도가 6.2 km/sec에서 7.9 km/sec로 속도가 급격히 변하고 있음에 비추어 Moho 불연속면은 심도 약 29 km에 존재하는 것으로 나타났다.